Coupled Diffusion and Adsorption Effects for Multiple Proteins in Agarose Gel

Jan Gutenwik, Bernt Nilsson, and Anders Axelsson
Dept. of Chemical Engineering I, Lund University, Lund, Sweden

DOI 10.1002/aic.10231
Published online in Wiley InterScience (www.interscience.wiley.com).

A mathematical model for the hindered diffusion and competitive adsorption of two proteins in an agarose gel has been developed. In a simulation program the model has been used to study the competing and displacement effects on a single bead for lysozyme and bovine serum albumin (BSA) bound to the ligand Cibacron Blue in agarose gel. The model takes into account hindered diffusion described by the Renkin model, competitive Langmuir adsorption kinetics, pore size distribution of the gel, and a shrinking effective pore radius attributed to molecule-to-ligand binding. The simulation model can easily explain displacement of BSA or lysozyme dependent on the binding capacity, kinetics, and diffusion. The influence of a bimodal pore size distribution is demonstrated. It also provides insight into the phenomenon of static vs. dynamic binding capacity observed in experimental determinations of the isotherm. © 2004 American Institute of Chemical Engineers *AIChE J,* 50: 3006–3018, 2004

Keywords: protein diffusion, dynamic simulation, modeling, lysozyme, BSA, agarose gel, hindered diffusion, competitive Langmuir adsorption kinetics, pore size distribution

Introduction

The separation of proteins is an important operation in the biotechnology industry as well as the pharmaceutical industry. It is most often carried out by some chromatographic process, affinity, ion-exchange, or hydrophobic interaction chromatography, which are commonly used. The development work often requires substantial input of experimental work, which is one of the reasons for the high costs in the development of new pharmaceuticals. It would therefore be of great help to make simulations in parallel with the experiments to obtain a better background for experimental planning and experimental work. If the simulation model at the same time provides a greater understanding of the underlying phenomena, there is an even greater gain. This is especially important because the separation of proteins includes several different competing effects that can be difficult to grasp without an organized approach as in a simulation model. Aspects that have to be included in this kind of model include a geometric description of the adsorbent matrix and competitive effects arising from different binding kinetics for the different proteins. These effects of hindered diffusion on protein transport in the gel network vary with time, molecular size of proteins, and gel properties. Furthermore, coupled effects of binding kinetics and diffusion develop, given that the bound protein molecules reduce the effective pore size and the available pore volume. This increases the hindrance effect along with the adsorption process.

The objective is to consider all these effects and to construct a simulation model with capability for process development and an increased understanding of the competing effects on the separation.

Models for one-component systems, taking into account hindered diffusion, pore size, and adsorption, are available.[1-8] McCoy et al.[9] developed a model describing the adsorption of adsorbate onto ligands on porous and nonporous particles in column systems. They took into account the adsorption and the adsorbing molecules occupying pore area, but did not consider the decrease in effective pore volume. Thus, their effective pore radius does not decrease. Clark et al.[10] described a decrease in pore radius when an enzyme is attached to the pore surface.

Correspondence concerning this article should be addressed to A. Axelsson at anders.axelsson@chemeng.lth.se.

For multicomponent protein adsorption, to our knowledge, no simulation studies have been done at the pore network level. Multicomponent effects are commonly studied at the column level.[11-13] Effects such as the displacement of proteins seen at column scale will probably also arise on the pore network scale in the beads.

The influence of the geometric properties of the gel is significant, although few data on this are available in the literature other than indirect measurements by gel chromatography. Normally this gives a value of the partition coefficient, but a measure of the pore size distribution can be obtained relating it to probe molecules such as poly(ethylene glycol) and dextran.[14,15] Interesting and useful work was done by Medin,[16] who made a thorough investigation of the structure of agarose. By using the scanning electron microscope technique, he found it to be bimodal, dividing the gel network into pores and microvoids. Bimodal pore size distributions are not uncommon. Loh et al.[17] studied pore size distributions using mercury intrusion experiments and found similar results for other porous media. Chiang et al.[18] compared different pore size distributions for enzyme loading. Li et al.19 calculated average pore diameters for agarose and alginate gels, giving an average pore diameter in good agreement with the data of Medin. Li et al.[19] also studied how the degree of crosslinking affected diffusion.

The structure of the gel can be modeled in different ways. Several authors have used a connectivity model.[1,3,4,6-8,17,20-22] The problem with advanced topological models is that they require detailed input of information such as adsorption measurements giving specific surface area and pore size distribution. This is possible if the adsorbent is sufficiently rigid, which is not the case for gels. Capillary models rely on fewer input data and give a fairly convenient description of the gel, which can provide sufficient information and understanding, although it should be kept in mind that problems can arise when the pore network is close to its percolation threshold. This is more easily dealt with in connectivity models.

Using the simulation model, the concentration gradients of adsorbed as well as free proteins can be generated. To validate these kinds of profiles there have, until now, been very few ways of doing this. However, the recent development of the confocal laser microscopy technique[23,24] opens up new possibilities here. In a previous study, confocal experiments were compared with a single protein system and showed promising results for future work in this field.[2]

A simulation program has been developed in this study. Although the present model has a simple physical description of the gel (Figure 1), it includes a variable diffusion coefficient and a variable porosity ascribed to a decrease in effective pore volume, considers a multiple dynamic adsorption–desorption process, and describes the wall effect for the diffusing protein molecules. Both diffusion and porosity are time dependent to fully describe the dynamic behavior of the coupled effects. In this way it is possible to study and understand the effect of hindered diffusion on the adsorption process in a fairly simple way. The aim is to use the model to increase understanding of a process containing too many parameters to be easily explained. Application of the model will also be used to discuss the difference in static and dynamic capacity often obtained experimentally.

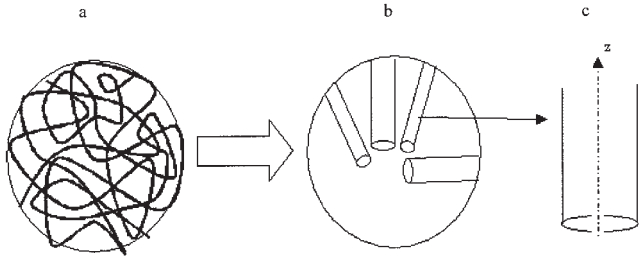

Figure 1. Simplification of the complex agarose network: (a) to a capillary pore distribution model; (b) to a single pore model (c).

Theory

Prediction of diffusion coefficients in liquid

One of the most common equations used to predict the diffusion coefficients in liquid is the Stokes–Einstein equation. It is derived for a sphere with radius R_S, moving in a fluid or continuum B.[25-28]

$$D_0 = \frac{RT}{6\pi\mu R_S N_A} = \frac{k_B T}{6\pi\mu R_S} \tag{1}$$

Here R is the ideal gas constant, T is the temperature, μ is the viscosity of the fluid, N_A is Avogadro's number, and R_S is the Stokes radius of the molecule. k_B is Boltzmann's constant, which is the quotient between ideal gas constant and Avogadro's number. The Stokes–Einstein equation is often used to obtain a rough estimate of the diffusion coefficient. In Eq. 1 a prediction of the diffusion coefficient in liquid was described. This gives an estimate of the diffusion coefficient based on the Stokes radius R_S and temperature T. The Stokes radius can be estimated from the molecular radius R_0, according to Fournier,[27] $R_S = R_0$

$$R_0 = \left(\frac{3M}{4\pi\rho N_A}\right)^{1/3} \tag{2}$$

where M is the molecular weight of the protein and ρ is the density of the molecule. This gives reasonable predictions of the diffusion coefficient in a dilute solution as long as no major conformational changes occur as a result of charges, for example. Several other predictive equations can be found in the literature.[9,18,19]

Prediction of hindered diffusion coefficients

Several methods have been developed to describe the variation of the diffusion coefficients attributed to the steric hindrances. One is the Renkin equation[19,29,30]

$$\frac{D}{D_0} = (1-\lambda)^2(1 - 2.104\lambda + 2.09\lambda^3 - 0.956\lambda^5) \tag{3}$$

The equation originates from the solution to the case of a spherical body falling in a liquid-filled pipe. As a general predictive model it is somewhat oversimplified, but for straight

cylindrical pores it has been shown to correlate well with experimental data.[30]

There are many other equations describing the correlation between the liquid diffusion coefficient and the hindered diffusion coefficient, such as Ogston's equation[30-36] or the Ferry–Faxén equation.[37,38]

Continuity equation

When molecules bind to the pore walls, the effective area of the pores decreases, thereby reducing the effective diffusion coefficient. Because it is not a constant during the period of time, all equations have to be based on the variable diffusion coefficient. The derivation of the continuity equation for one of the proteins is shown below. Similar equations are obtained for each protein. They can be derived from mass balances, as follows

$$\text{In} - \text{Out} = \text{Accumulation} - \text{Production} \tag{4}$$

In − Out

$$-\partial\left[A\varepsilon_r\left(-D\frac{\partial C_A}{\partial z}\right)\right] \tag{5}$$

Accumulation

$$\frac{\partial m}{\partial t} = \frac{\partial (VC_A)}{\partial t} = V\frac{\partial C_A}{\partial t} + C\frac{\partial V}{\partial t} \tag{6}$$

Production

$$-A\partial z r_A \tag{7}$$

Insertion of Eqs. 5–7 into Eq. 4 yields

$$V\frac{\partial C_A}{\partial t} + C\frac{\partial V}{\partial t} = -\partial\left[A\varepsilon_r\left(-D\frac{\partial C_A}{\partial z}\right)\right] - A\partial z r_A \tag{8}$$

where

$$V = A\varepsilon_r\partial z \tag{9}$$

$$A\varepsilon_r\partial z\frac{\partial C_A}{\partial t} + C_A\frac{\partial (A\varepsilon_r\partial z)}{\partial t} = -\partial\left[A\varepsilon_r\left(-D\frac{\partial C_A}{\partial z}\right)\right] - A\partial z r_A \tag{10}$$

Because A and dz are constants, the above equation can be derived as follows

$$\frac{\partial C_A}{\partial t} + \frac{C_A}{\varepsilon_r}\frac{\partial \varepsilon_r}{\partial t} = -\frac{1}{\varepsilon_r}\frac{\partial}{\partial z}\left[\varepsilon_r\left(-D\frac{\partial C_A}{\partial z}\right)\right] - \frac{r_A}{\varepsilon_r} \tag{11}$$

C_A, ε_r, and D all depend on both time and position in the pore, thereby differentiating with respect to the position in the pore, giving three terms from the production term

$$\frac{\partial C_A}{\partial t} + \frac{C_A}{\varepsilon_r}\frac{\partial \varepsilon_r}{\partial t} = \frac{1}{\varepsilon_r}\left(D\frac{\partial C_A}{\partial z}\frac{\partial \varepsilon_r}{\partial z} + \varepsilon_r\frac{\partial C_A}{\partial z}\frac{\partial D}{\partial z} + \varepsilon_r D\frac{\partial^2 C_A}{\partial z^2}\right) - \frac{r_A}{\varepsilon_r} \tag{12}$$

Rearranging gives

$$\frac{\partial C_A}{\partial t} = -\frac{C_A}{\varepsilon_r}\frac{\partial \varepsilon_r}{\partial t} + \frac{D}{\varepsilon_r}\frac{\partial C_A}{\partial z}\frac{\partial \varepsilon_r}{\partial z} + \frac{\partial C_A}{\partial z}\frac{\partial D}{\partial z} + D\frac{\partial^2 C_A}{\partial z^2} - \frac{r_A}{\varepsilon_r} \tag{13}$$

In Eq. 13 there are several time derivatives and unknown space derivatives, which need to be expressed

$$\frac{\partial \varepsilon_r}{\partial t} = \frac{\partial \varepsilon_r}{\partial r}\frac{\partial r}{\partial t} \tag{14}$$

ε_r is defined as actual pore volume divided by starting pore volume as

$$\varepsilon_r = \frac{\pi r^2\partial z}{\pi R_{pore}^2\partial z} = \frac{r^2}{R_{pore}^2} \tag{15}$$

and differentiated with respect to the pore radius gives

$$\frac{\partial \varepsilon_r}{\partial r} = \frac{2r}{R_{pore}^2} \tag{16}$$

The derivation of the term $\partial r/\partial t$ is slightly more complicated. The annular volume V between two cylinders is given by

$$V = h\pi(R_{pore}^2 - r^2) \tag{17}$$

and describes the total volume occupied by molecules in a segment of the pore. Thus, the radius changes from R_{pore} to r. The same volume can also be expressed in terms of the molecules that are bound to the ligands within the volume of the segment

$$V = \left(\frac{4\pi R_0^3}{3}\right)qh\pi R_{pore}^2 N_A \tag{18}$$

Insertion of Eq. 17 into Eq. 18, and rearranging, gives

$$r = \left[R_{pore}^2 - \left(\frac{4\pi R_0^3}{3}\right)\frac{qh\pi R_{pore}^2 N_A}{h\pi}\right]^{0.5} \tag{19}$$

Equation 19 gives the actual pore radius when a certain number of protein molecules have been adsorbed (q), where only q is a function of time. Differentiating with respect to time gives the following:

$$\frac{\partial r}{\partial t} = \frac{-0.5\left(\frac{4\pi R_0^3}{3}\right)R_{pore}^2 N_A}{\left[R_{pore}^2 - \left(\frac{4\pi R_0^3}{3}\right)qR_{pore}^2 N_A\right]^{0.5}} \frac{\partial q}{\partial t} \tag{20}$$

where $\partial q/\partial t$ follows the competitive Langmuir kinetics for multiple proteins[11,39,40]

$$-r_A = \frac{\partial q}{\partial t} = k_{adsA} C_A q_{\max A}\left(1 - \frac{q_A}{q_{\max A}} - \frac{q_B}{q_{\max B}}\right) - k_{desA} q_A \tag{21}$$

where $q_{\max A}$ is derived from experimental data and scaled according to Gutenwik et al.[2] When the left-hand side in Eq. 21 is zero, the system has attained equilibrium. Then the equation can be rewritten according to

$$\frac{q_A}{q_{\max A}} = \frac{C_A \frac{k_{adsA}}{k_{desA}}}{1 + C_A \frac{k_{adsA}}{k_{desA}} + C_B \frac{k_{adsB}}{k_{desB}}} \tag{22}$$

for molecule A, and a similar equation for B, by exchanging index.

Boundary conditions

The boundary condition between the bulk and the interface for the concentration is given by an external mass transfer coefficient. This was derived in a previous work[2]

$$D \frac{\partial C_A}{\partial z} = -K_{mass}(C_{A_{\text{in}}} - C_{A_{\text{boundary}}}) \qquad \text{at } z = 0 \tag{23}$$

In the center of the bead the derivative of the concentration is 0, attributed to the symmetry effect

$$D \frac{\partial C_A}{\partial z} = 0 \qquad \text{at } z = L \tag{24}$$

The derivatives of ε_r and D are given as numerical derivatives at the interface and from the symmetry effect in the center of the bead.

Pore size distribution

This study uses cylindrical pores to describe the complex structure of agarose gel. It is based on the measurements of pore size distribution by Medin.[16] It is clearly seen there that the structure of agarose is bimodal, with large microvoids (diameter 100–600 nm) and smaller pores (diameter 10–100 nm). In the simulation, however, these distributions are replaced by Gaussian distributions because of the ease of simulating and changing parameters.

The two Gaussian distributions describe the microvoids and pores shown by Medin.[16]

Each distribution is then divided into different classes. When the pores are added together to describe a bead, they are scaled with this distribution, but also scaled by the volume, given that the volume is greater at the surface than in the center of the beads. This means that there are more pores at the surface, although the porosity and distribution are the same in the whole bead.

Table 1. Physical Data for Lysozyme and BSA

Protein	Molecular Weight (g/mol)	Stokes Radius (nm)	Diffusivity, $D_0 \times 10^{11}$ (m^2/s)	
Lysozyme	14,800	1.8*	12**	11.8†
BSA	66,000	3.0*	7.1**	5.9†

* Calculated from Eq. 2.
**Calculated from Eq. 1.
† From Tyn and Gusek.[44]

Materials and Methods

Porous media

When studying diffusion in agarose gels, it is very important to know the distribution of the pores. Medin[16] studied the pore size distribution in 2, 3, and 4% agarose gels. The pores are divided into two classes, pores and microvoids. The range of pore diameters is from 10 to 100 nm, whereas the range for microvoids is 100 to 600 nm. In the present study a 4% (w/w) agarose gel has been simulated. However, the model is general and can easily be used to simulate any gel.

Proteins

To simulate realistic molecules two different molecules have been used: lysozyme and bovine serum albumin (BSA). These are well known and commonly used proteins, and it is thus easy to compare results. Some data regarding these molecules can be found in Table 1. The effect of protein charge is not taken into account in the model to elucidate the pure effects of adsorption kinetics and diffusion.

Ligands

The protein molecules bind to different ligands. In this study Cibacron Blue was used as ligand for lysozyme and BSA. However, in some of the comparative simulations the same adsorption kinetics as for lysozyme were used for both model molecules, to elucidate and analyze the effects of hindered diffusion. Adsorption kinetic parameters are summarized in Table 2.

Numerical method

The model is described by a parabolic partial differential equation (PDE), with an associated adsorption kinetic equation. It is solved by the method of lines based on finite-difference approximations of the space dimension (that is, the pore length). This is discretized into grid points. The approximation results in a large set of ordinary differential equations (ODEs) in time, which are solved with an implicit ODEsolver (in our case ode15s).[41] Base case parameters and protein data used in the simulations are given in Table 2 and Table 1, respectively. Some of the data have been varied in the parameter study to observe the effects of specific parameters.

Table 2. Base Case Parameters Used in the Simulations*

Base Case Parameter	Value
C_{Ain}	7.14×10^{-3} mol/m^3
k_{ads} lysozyme	1.144 m^3/(mol s)
k_{ads} BSA	5.72 m^3/(mol s)
k_{des} lysozyme	2.0×10^{-3} (1/s)
k_{des} BSA	1.0×10^{-2} (1/s)
L	0.5×10^{-4} m
q_{max} lysozyme	1 mol/m^3 sedimented gel
q_{max} BSA	0.1 mol/m^3 sedimented gel
R_{pore} microvoids	50–200 nm
R_{pore} pores	10–30 nm
T	293 K
ε_{bead}	0.75
ε_{bed}	0.37
μ	1005×10^{-6} Pa · s

*Protein data according to Table 1.

Results and Discussion

The combined effect of the competitive adsorption of the two proteins and the hindered diffusion for the respective protein, which changes as a result of the adsorption, is difficult to predict. The effective pore radius available for the diffusive transport decreases because of the steric hindrance induced by the adsorption of the protein molecules. This is investigated by a parameter study in which the contributions from different parameters can be seen.

To make a realistic comparison, experimental data for kinetics, binding capacity, and diffusion coefficients have been used. Experimental data have been obtained from Carlsson[42] and Persson et al.[43] and are given in Table 2. This illustrates the base case.

The parameter study is made for four different cases besides the experimental base case according to Table 3. In the study, the lysozyme kinetics is kept constant in all cases and the influence of changes in BSA parameters is studied.

It should be noted here what is meant by "equilibrium." This is not as trivial as it might seem, because there are two different kinds of equilibrium, one where the molecules in the solution strive for equilibrium with the bound molecules according to the adsorption kinetics, and one where the concentration in the solution strives to reduce the concentration gradient in the whole pore. Moreover, when the values of bound proteins are normalized, the value used is when both equilibriums are fulfilled. The equilibrium state referred to in the following discussion is attained when $dq/dt = 0$ as well as $dc/dt = 0$ throughout each pore. This means that the protein is bound according to the equilibrium isotherm and that there is no axial concentration gradient in the pore liquid. The q-values of bound protein are normalized with this equilibrium case.

Influence of hindered diffusion (Figures 2 and 3)

The influence of hindered diffusion is illustrated in Figure 2, which shows the isokinetic case where the binding kinetics is the same for both proteins and equal to that of lysozyme. The diffusion coefficients vary because of their size and effective pore radius according to Eq. 3. This is obviously not a realistic case, but merely a measure for comparison and to isolate the influence of diffusion only.

The concentration profiles for the adsorbed amount of protein as a function of pore length and time are presented in the same graph for ease of comparison. The adsorbed amount of each protein q is normalized with its equilibrium value of bound protein for the given inlet bulk concentration. This means that the q-value will attain unity for both proteins after sufficient time.

It is evident that the smaller lysozyme molecules diffuse faster than the larger BSA molecules. A displacement effect can be seen for lysozyme. Because lysozyme is smaller than BSA, it diffuses faster and thereby reaches the binding sites inside the pores faster. Thus, lysozyme can bind to more sites than they can when there is competitive equilibrium where both proteins are present at full concentration. This explains the values higher than unity for lysozyme, and also explains the displacement phenomenon. As BSA concentration catches up, it will compete with lysozyme for the binding sites, thereby pushing lysozyme ahead and increasing the concentration in the inner volume layer. This can be seen as a peak in the lysozyme concentration, starting at 0.3 h moving inward with time.

When comparing the total accumulated amount of bound proteins, the difference in volume between different layers in the bead must be taken into account. This effect can be seen in Figure 3, where the total amount of bound protein is given as a function of time. Figure 3 also illustrates that lysozyme diffuses faster and thereby binds faster, which leads to the displacement effect and eventually the decrease in the amount of bound protein.

Influence of kinetics (Figure 4)

When increasing both the adsorption and the desorption rate constants (k_{ads} and k_{des}) by a factor of 5 for BSA as compared to lysozyme, the concentration profiles for the adsorbed proteins in the bead are obtained according to Figure 4. There is a very small difference compared to the isokinetic case in Figure 2, which indicates that the adsorption kinetics is very fast compared to the diffusion already in the first case (Figure 2). Only a slightly steeper gradient is obtained. This creates a slightly more shrinking core effect than that in the previous case.

From these two simulations it can be concluded that it would be a good approximation to use the adsorption isotherm instead of using the Langmuir rate expression in the model. This illustrates that this type of simulations can be used for model simplification in the modeling of chromatography separations.

Table 3. The Different Cases Used in the Parameter Study

Case	Description	Figure
1	Isokinetic case. Lysozyme data from Table 2 used for both lysozyme and BSA	2, 3, and 9
2	k_{ads} and k_{des} increased 5 times for BSA compared to case 1	4
3	k_{ads} increased 2 times for BSA compared to case 1	5 and 6
4	q_{max} decreased 10 times for BSA compared to case 1	7
5	Experimental base case. All changes from cases 2–4	8 and 10

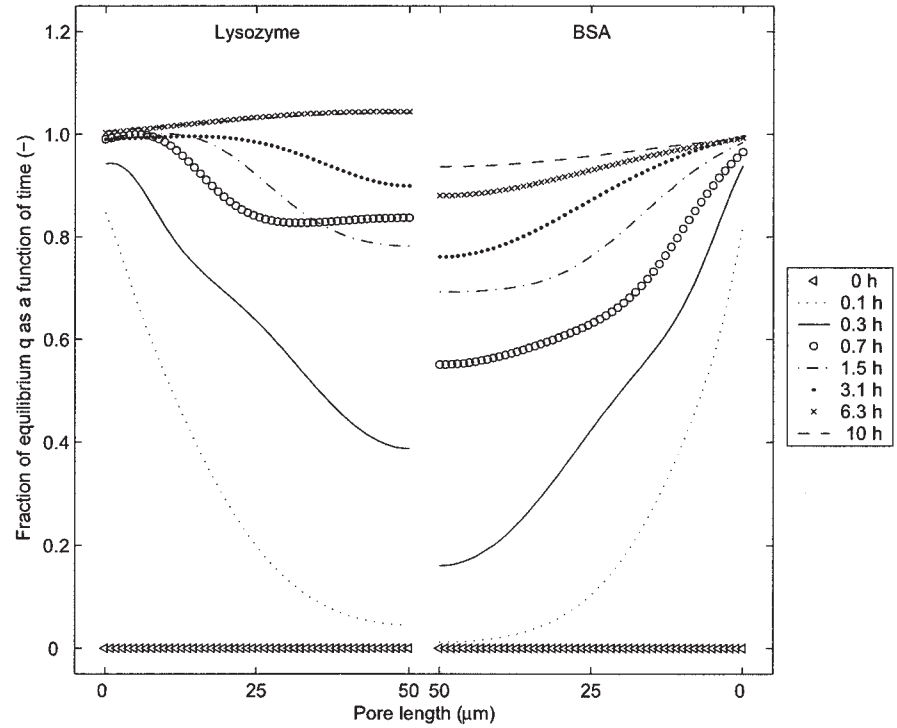

Figure 2. Fraction of equilibrium *q* as a function of time and bead position for lysozyme and BSA.

Note that the two proteins are normalized with their q_{max} and competitive Langmuir isotherm; thus at equilibrium they will reach unity. However, this does not say anything about the actual amount of bound protein.

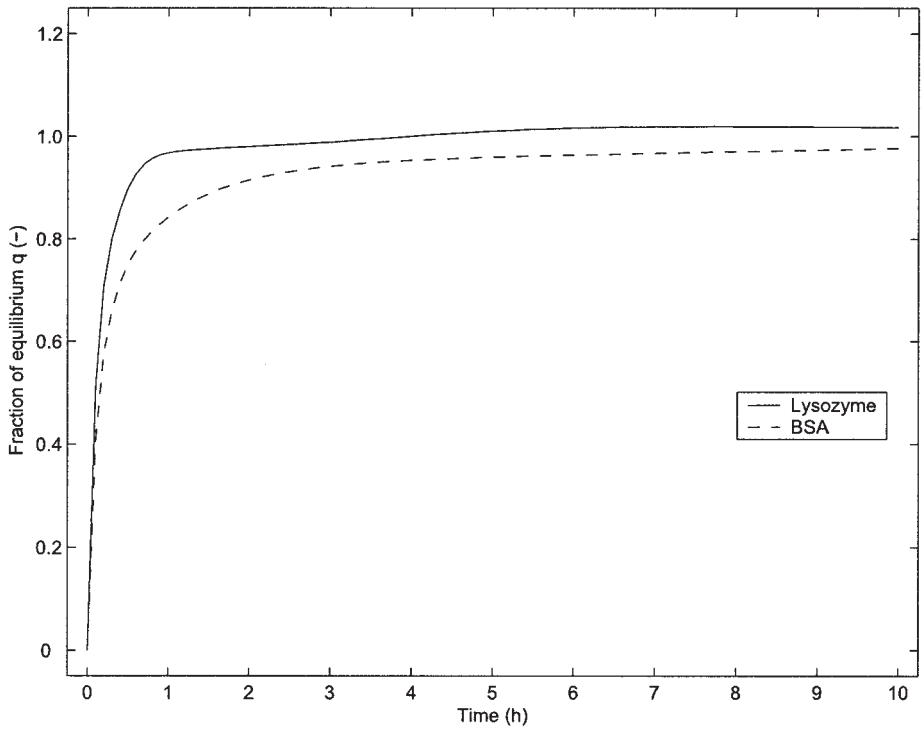

Figure 3. Accumulated normalized fraction of *q* as a function of time for the whole bead.

Note that the two proteins are normalized with their q_{max} and competitive Langmuir isotherm; thus at equilibrium they will reach unity. However, this does not say anything about the actual amount of bound protein.

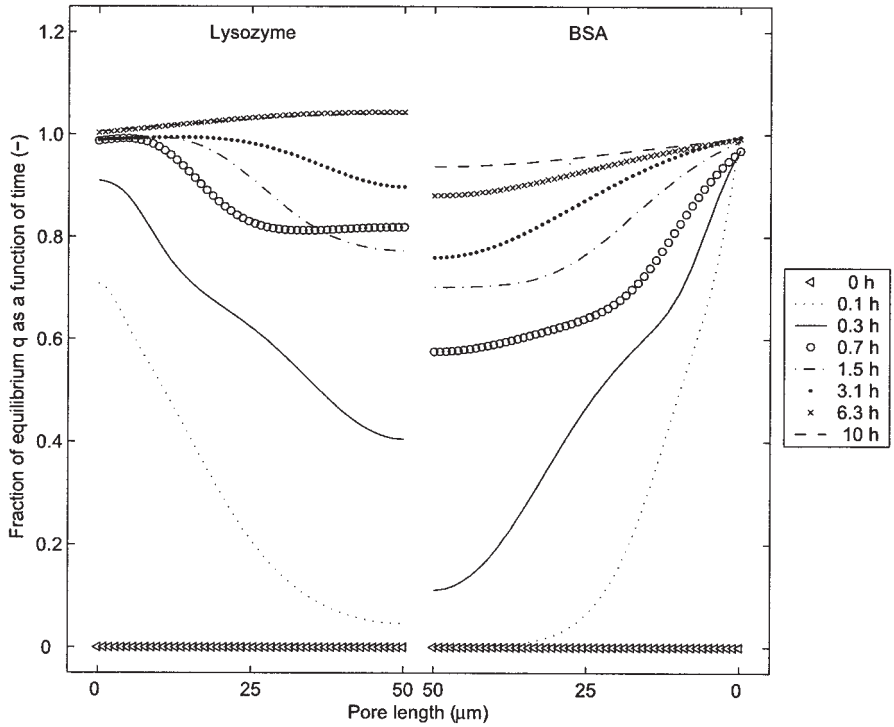

Figure 4. Fraction of equilibrium *q* as a function of time and bead position for lysozyme and BSA.

Increased adsorption and desorption kinetics by a factor of 5 for BSA. Note that the two proteins are normalized with their q_{max} and competitive Langmuir isotherm; thus at equilibrium they will reach unity. However, this does not say anything about the actual amount of bound protein.

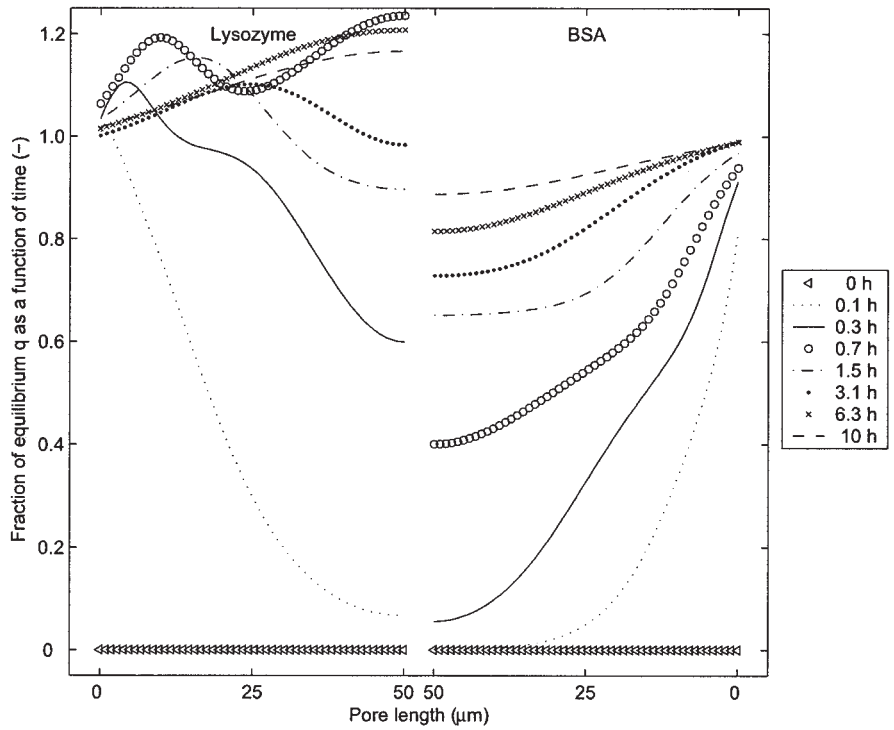

Figure 5. Fraction of equilibrium *q* as a function of time and bead position for lysozyme and BSA.

Increased adsorption kinetics by a factor of 2 for BSA. Note that the two proteins are normalized with their q_m and competitive Langmuir isotherm; thus at equilibrium they will reach unity. However, this does not say anything about the actual amount of bound protein.

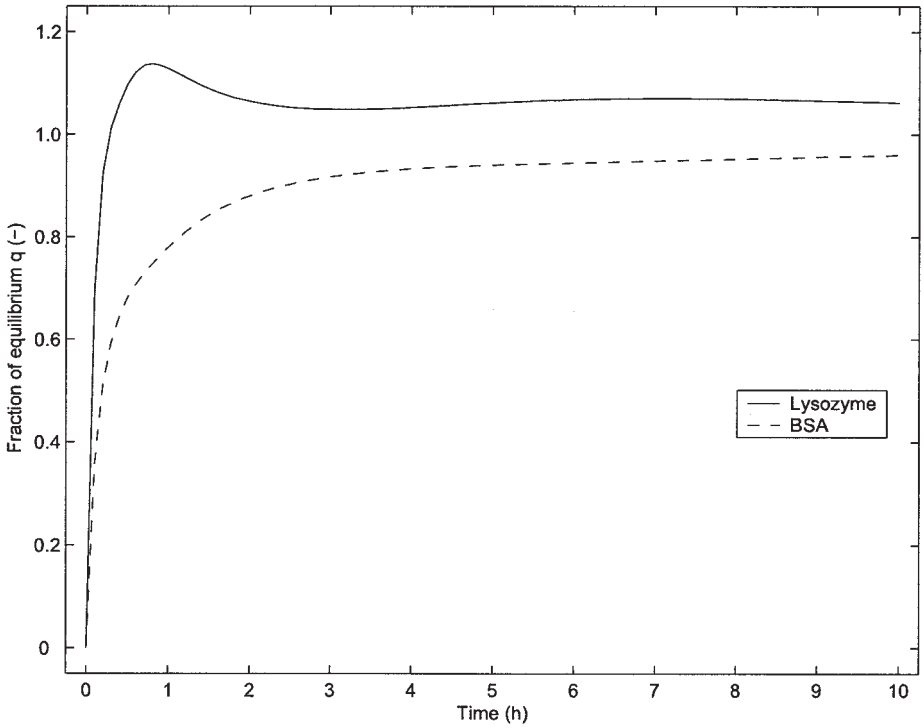

Figure 6. Accumulated normalized fraction of q as a function of time for the whole bead.

Increased adsorption kinetics by a factor of 2 for BSA. Note that the two proteins are normalized with their q_{max} and competitive Langmuir isotherm; thus at equilibrium they will reach unity. However, this does not say anything about the actual amount of bound protein.

Influence of association constant (Figures 5 and 6)

The association constant k_{ads}/k_{des} is increased by a factor of 2 for BSA by increasing k_{ads} by a factor of 2, while keeping all other parameters the same as in the isokinetic case. This results in a considerable change, which can be seen in Figure 5. Thus, the adsorption rate has been doubled for BSA, whereas the desorption rate is the same.

This changes the relationship between the binding capacities for the two proteins according to the Langmuir isotherm (see Eq. 22), which explains why the displacement peak is larger for this case than that in the isokinetic case (Figure 2). At the beginning, the concentration of lysozyme is greater than that of BSA because of faster diffusion. Thus lysozyme binds to more sites than is given by the equilibrium. Because the equilibrium value of q for lysozyme is lower, compared to the isokinetic case, more lysozyme molecules are displaced when the BSA molecules catch up.

An interesting and, at first sight, unexpected phenomenon can be seen in the center of the bead. From 0.7 to 1.5 h the amount of bound protein decreases for lysozyme in the center of the bead. This was already seen in the first isokinetic case (Figure 2) but is accentuated in Figure 5 where the amount of bound protein decreases from a concentration high above equilibrium to a concentration below equilibrium. This will be discussed later in the section discussing the influence of pore size distribution.

In Figure 6 the accumulated amount of protein adsorbed, for the case in Figure 5, is shown as a function of time (similar to Figure 3). After about 1 h there is a peak in the lysozyme concentration, which is attributed to the decrease in volume. Thus, when a molecule is displaced from an outer layer, there are not as many binding sites inside because of the smaller volume. Therefore the total amount of the bound lysozyme molecules decreases, resulting from the displacement effect, although the protein still increases to bind further inside the bead. The displacement effect obtained is greater when the association constant is increased. Thus, the peak is more significant in Figure 6 compared to Figure 3, where the peak can be observed only after a careful inspection.

Influence of loading capacity (Figure 7)

In Figure 7 the loading capacity q_{max} for BSA has instead been decreased by a factor of 10. A lower loading capacity is reasonable for a larger molecule because of the hindrance effects, where each molecule can block sites not occupied by proteins. Experimental determination of the loading capacity has shown that the decrease is of the order of 10 times lower for BSA than for lysozyme in the present system.[43] This means that BSA does not have to bind to as many ligands as lysozyme to reach equilibrium. Because the same concentration is used BSA will attain equilibrium faster. This explains why the concentration profiles for BSA attain unity much faster than lysozyme in Figure 7. It should be noted that the equilibrium is defined as the equilibrium after a long time, when the pore concentration is the same in the whole bead. Thus, the normalized loading capacity can be higher than unity for one of the proteins. However, it cannot of course be higher than the isothermal equilibrium for one component. Because BSA occupies its binding sites faster than lysozyme, it also will occupy binding sites, which will be available for lysozyme when its

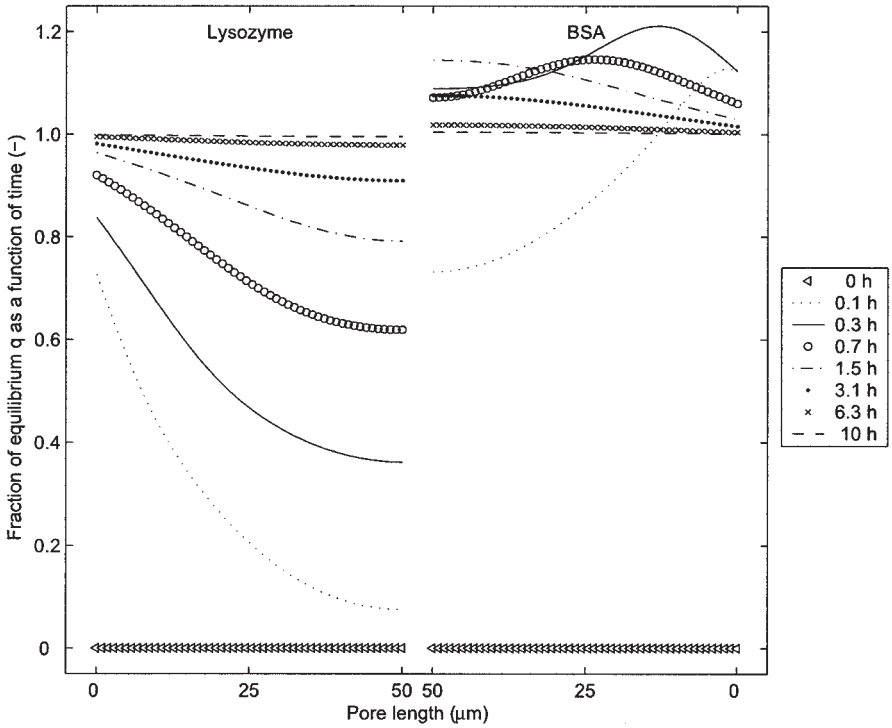

Figure 7. Fraction of equilibrium *q* as a function of time and bead position for lysozyme and BSA.

Decreased maximum loading capacity by a factor of 10 for BSA, q_{maxB}. Note that the two proteins are normalized with their q_{max} and competitive Langmuir isotherm; thus at equilibrium they will reach unity. However, this does not say anything about the actual amount of bound protein.

concentration is sufficient. In this way BSA will be displaced by lysozyme, which is quite the reverse of the case discussed in Figures 2–5.

Experimental base case (Figure 8)

When all these studied effects are considered together, we end up with the true relation between lysozyme and BSA, which is illustrated by Figure 8. It can be seen that the influence of q_{max} is most important because this determines whether lysozyme or BSA will be displaced. It can partly be explained by the fact that at a low binding capacity an excess of protein molecules will be available in the pore liquid. Thus, equilibrium is attained much faster. However, this is not the whole truth. If so, this would be accomplished only by changing the inlet concentration to the pore. However, this does not change the displacement order.

Influence of pore size distribution

As mentioned earlier, it was observed that the center concentration of adsorbed lysozyme showed peculiar behavior over time. First it increases, followed by a slight decrease (from 0.7 h to 1.5 h in the present cases), and finally it increases up to the final equilibrium value (see Figure 2 and especially Figure 5).

This is most effectively explained by illustrating the adsorbed lysozyme concentration in the bead center as a function of time in relation to the three-dimensional isotherm. In Figure 9 the competitive adsorption isotherm for BSA and lysozyme is shown as a shaded surface, for the isokinetic case (described earlier in the section on influence of hindered diffusion), where the adsorbed amount of lysozyme is plotted against the BSA and lysozyme concentrations in the liquid. The adsorbed amount of lysozyme is normalized with the maximum loading capacity $q_{\max\ lys}$, defined in Eq. 22. This normalization is different from that used in Figures 2–8 to show more clearly the adsorbed amount of lysozyme in relation to the equilibrium conditions during the adsorption process.

At the front, at a zero BSA concentration in the liquid, the one-component isotherm for lysozyme can be seen as a limit curve for the shaded isotherm area. At the rear, at a normalized BSA concentration of unity, another isotherm for lysozyme with BSA present at full concentration can be seen as another limit curve.

In Figure 9 the time history for the concentration of lysozyme in the center of the bead is illustrated by the dashed and solid lines, starting at zero concentration of BSA and lysozyme in the liquid. The adsorbed concentration of lysozyme follows the solid line with time to the end point where the adsorbed amount of lysozyme has increased to its final value. The dashed line illustrates the true equilibrium conditions during the same time.

Because lysozyme diffuses faster, it increases in concentration at the beginning, thereby being able to bind to a greater number of sites than would be possible at equilibrium. Then slowly BSA catches up, increases in concentration and competes with lysozyme for available binding sites. Thus, lysozyme is displaced, and the adsorbed fraction of lysozyme decreases. This is followed by an increase, which depends on the bimodal distribution of pores and the greater diffusion

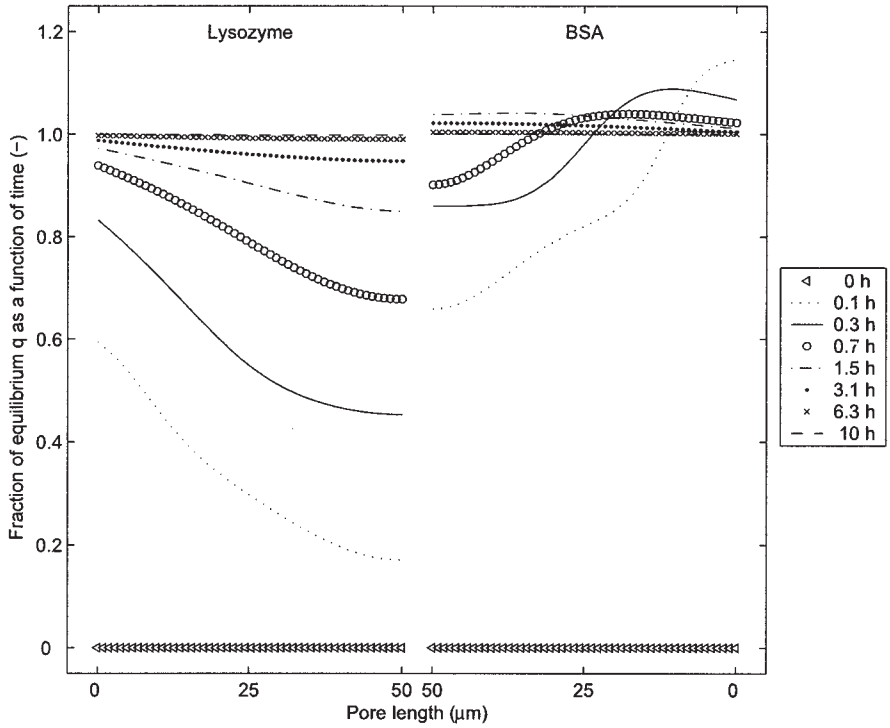

Figure 8. Fraction of equilibrium *q* as a function of time and bead position for lysozyme and BSA, using the experimentally determined values for BSA and lysozyme.

Note that the two proteins are normalized with their q_{max} and competitive Langmuir isotherm; thus at equilibrium they will reach unity. However, this does not say anything about the actual amount of bound protein.

hindrance in the small pores. This is seen as the extra curvature in the solid concentration–time curve. Thus, the concentration of lysozyme increases again when the small pores also become filled, which is followed by another decrease when BSA fills the small pores.

The importance of the adsorption kinetics can also be studied

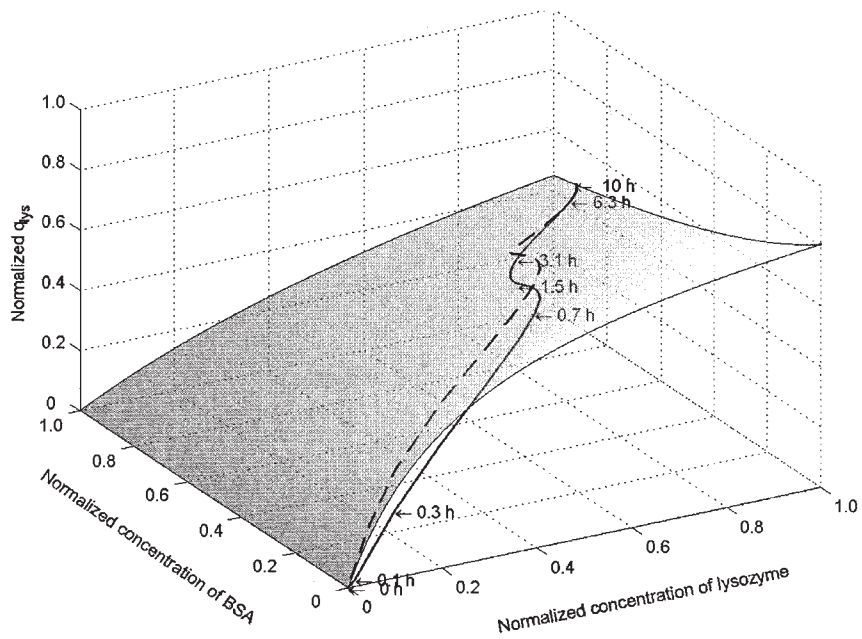

Figure 9. Normalized amount of bound lysozyme in the end of the pore as a function of concentration of lysozyme and BSA.

The shaded surface shows the isotherms for all concentrations of lysozyme and BSA. The dashed line represents the isotherm (that is, the true equilibrium) for the concentrations in the end of the pore as a function of time, whereas the solid line represents the actual amount given by the model of bound lysozyme.

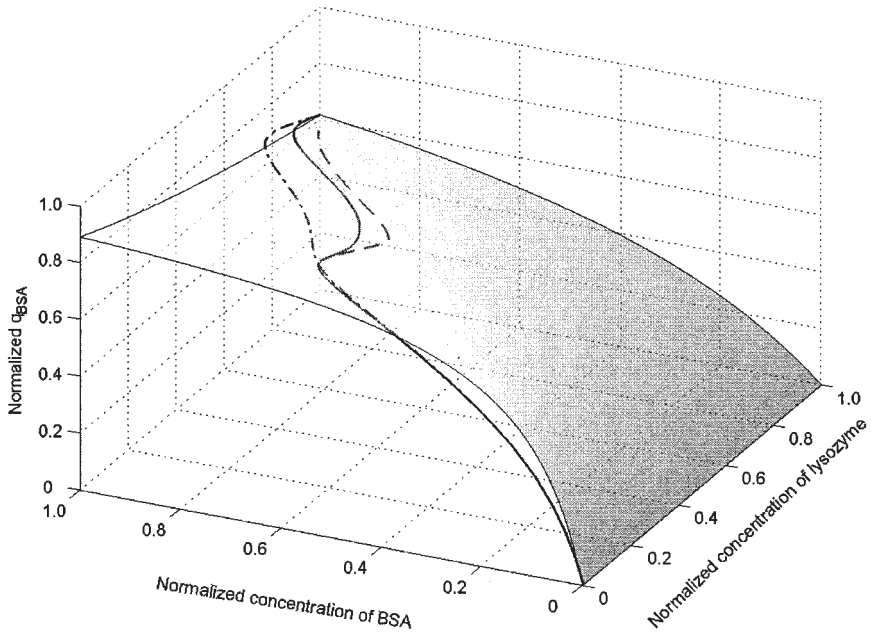

Figure 10. Normalized amount of bound BSA in the end of the pore as a function of concentration of lysozyme and BSA.

The shaded surface shows the isotherms for all concentrations of lysozyme and BSA. The lines represent different distributions of the small pores. The solid line represents the actual distribution given by Medin (10–30 nm). The dash-dotted line represents a larger distribution of the small pores (20–60 nm) and the dashed line represents smaller distribution (5–15 nm). The same total pore volume is used.

in Figure 9, where the solid line describes the value when using adsorption kinetics and the dashed line represents calculated values for the isotherm. The vertical difference between the dashed and solid lines illustrates the driving force for the adsorption.

To further investigate the influence of the hindered diffusion in the small pores a similar three-dimensional figure (as in Figure 9) of the adsorbed amount of BSA as a function of the lysozyme and BSA concentrations in the liquid is presented in Figure 10. Again the isotherm surface can be seen as the shaded surface. The distribution of the small pores was varied from their original size of 10–30 nm in radius by increasing and decreasing the mean size by a factor of 2 (5–15 and 20–60 nm). The three different cases are illustrated by the three curves giving the time history of the adsorbed amount of BSA in the center of the bead. For the larger size distribution the S-shape diminishes, whereas the curvature is greatly increased for the smaller pore distribution. Thus, it is obvious that the S-shape of the curve depends on the bimodal distribution, but also on the ratio between the size of the pores and the molecules. When the ratio between the pore radius and the molecule radius is greater than a factor of 10, the hindrance effect is small because of the interaction with the pore walls. When the pore mean size decreases the hindrance effect is greater, and the curve consequently becomes more nearly S-shaped and a plateau is formed. This decrease in diffusion coefficient is one explanation for why there is often a difference in the static and dynamic loading capacity when performing chromatography experiments. The dynamic measurements in a chromatography column operate on a shorter timescale and it appears that an equilibrium is attained fairly soon. The very different timescale for filling the small pores as compared to the large pores is therefore not considered in the dynamic measurements.

Conclusions

In this study a mathematical model for the hindered diffusion and adsorption of two proteins in an agarose gel has been developed. In a simulation program the model has been used to study the competing and displacement effects on a single bead. The model takes into account: (1) hindered diffusion described by the Renkin equation, (2) competitive Langmuir adsorption kinetics, (3) pore size distributions of the gel, and (4) a shrinking effective pore radius resulting from molecule-to-ligand binding.

The model system used in this study constitutes affinity adsorption of lysozyme and BSA to Cibacron Blue in agarose gel beads. From generated concentration profiles it is fairly easy to explain the competition and displacement attributed to the combined effects of hindered diffusion, adsorption kinetics, and binding capacities. It also provides insight into the phenomenon of static vs. dynamic binding capacity.

The model is general and the simulation program can easily be used to simulate any molecules in any adsorption matrix as long as experimental adsorption kinetics data and gel pore size data are available or can be estimated.

The model is well suited for parameter studies to be used for a deeper understanding of the rate-determining steps and mechanisms. A future application of the simulation program is to compare simulations with experimental confocal measurements on multicomponent systems.

Notation

A = area, m^2
C_A = concentration in the pore, mol/m^3
D = diffusion coefficient, m^2/s
h = length of a segment in the pore, m

K_{mass} = external mass transfer coefficient, m/s
k_{ads} = adsorption rate coefficient, $m^3\ mol^{-1}\ s^{-1}$
k_B = Boltzmann's constant, J/K
k_{des} = desorption rate coefficient, s^{-1}
L = length of pore, m
M = molecular weight, g/mol
m = mass of element, kg
N_A = Avogadro's number, mol^{-1}
q = amount of bound ligands, mol/m^3 pore
q_{max} = total amount of ligands, mol/m^3 pore
R = universal gas constant, $J\ K^{-1}\ mol^{-1}$
R = molecular radius, m
R_{pore} = pore radius, m
r = effective pore radius, m
r_A = rate of adsorption/desorption, mol/m^3 pores s^{-1}
T = temperature, K
t = time, s
V = volume, m^3
z = length coordinate of pore, m

Greek letters

ε = porosity
ε_{bead} = porosity of the bead
ε_{bed} = porosity of the bed
ε_r = shrinking pore coefficient (actual pore volume/total pore volume)
λ = ratio between molecule radius and pore radius
μ = dynamic viscosity, Pa·s
ρ = density of molecule, kg/m^3

Subscripts

A = component A
B = component B
boundary = boundary or interface
e = effective
0 = initial or pure state
in = inlet or bulk

Literature Cited

1. Bryntesson LM. Pore network modelling of the behaviour of a solute in chromatography media: Transient and steady-state diffusion properties. *Journal of Chromatography A.* 2002;945:103-115.
2. Gutenwik J, Nilsson B, Axelsson A. Effect of hindered diffusion on the adsorption of proteins in agarose using a pore model. *Journal of Chromatography A.* 2004;1048:161-172.
3. Liapis AI, Meyers JJ, Crosser OK. Modeling and simulation of the dynamic behavior of monoliths effects of pore structure from pore network model analysis and comparison with columns packed with porous spherical particles. *Journal of Chromatography A.* 1999;865: 13-25.
4. Meyers JJ, Liapis AI. Network modeling of the intraparticle convection and diffusion of molecules in porous particles packed in a chromatographic column. *Journal of Chromatography A.* 1998;827:197-213.
5. Meyers JJ, Nahar S, Ludlow DK, Liapis AI. Determination of the pore connectivity and pore size distribution and pore spatial distribution of porous chromatographic particles from nitrogen sorption measurements and pore network modelling theory. *Journal of Chromatography A.* 2001;907:57-71.
6. Meyers JJ, Crosser OK, Liapis AI. Pore network modelling: Determination of the dynamic profiles of the pore diffusivity and its effect on column performance as the loading of the solute in the adsorbed phase varies with time. *Journal of Chromatography A.* 2001;908:35-47.
7. Meyers JJ, Crosser OK, Liapis AI. Pore network modelling of affinity chromatography: Determination of the dynamic profiles of the pore diffusivity of B-galactosidase and its effect on the column performance as the loading of B-galactosidase onto anti-B-galactosidase varies with time. *Journal of Biochemical and Biophysical Methods.* 2001;49:123-139.
8. Petropoulos JH, Liapis AI, Kolliopoulos NP, Petrou JK, Kanellopoulos NK. Restricted diffusion of molecules in porous affinity chromatography adsorbents. *Bioseparation.* 1990;1:69-88.
9. McCoy MA, Liapis AI. Evaluation of kinetic models for biospecific adsorption and its implications for finite bath and column performance. *Journal of Chromatography.* 1991;548:25-60.
10. Clark DS, Bailey JE, Do DD. A mathematical model for restricted diffusion effects on macromolecule impregnation in porous supports. *Biotechnology and Bioengineering.* 1985;27:208-213.
11. Fargues C, Bailly M, Grevillot G. Adsorption of BSA and hemoglobin on hydroxyapatite support: Equilibria and multicomponent dynamic adsorption. *Adsorption.* 1998;4:5-16.
12. Gallant SR, Kundu A, Cramer SM. Modeling non-linear elution of proteins in ion-exchange chromatography. *Journal of Chromatography A.* 1995;702:125-142.
13. Heeter GA, Liapis AI. Multi-component perfusion chromatography in fixed bed and periodic current column operation. *Journal of Chromatography A.* 1996;734:105-123.
14. Andersson M, Axelsson A, Zacchi G. Determination of the pore-size distribution in gels. *Bioseparation.* 1995;5:65-72.
15. Hagel L, Östberg M, Andersson T. Apparent pore size distribution of chromatography media. *Journal of Chromatography A.* 1996;743:33-42.
16. Medin A. Studies on structures and properties of agarose. PhD Thesis. Uppsala University, Uppsala, Sweden; 1995.
17. Loh KC, Wang DIC. Characterization of pore size distribution of packing materials used in perfusion chromatography using a network model. *Journal of Chromatography A.* 1995;718:239-255.
18. Chiang CL, Wu TC, Wang YJ. Enzyme loading in a solid support with nonuniform pore size distribution. *Biotechnology and Bioengineering.* 1990;35:976-982.
19. Li RH, Altreuter DH, Gentile FT. Transport characterization of hydrogel matrices for cell encapsulation. *Biotechnology and Bioengineering.* 1996;50:365-373.
20. Grimes BA, Meyers JJ, Liapis AI. Determination of the intraparticle electroosmotic volumetric flow-rate, velocity and Peclet number in capillary electrochromatography from pore network theory. *Journal of Chromatography A.* 2000;890:61-72.
21. Meyers JJ, Liapis AI. Network modeling of the convective flow and diffusion of molecules adsorbing in monoliths and in porous particles packed in a chromatographic column. *Journal of Chromatography A.* 1999;852:3-23.
22. Nicholson D, Petrou JK, Petropoulos JH. Relation between macroscopic conductance and microscopic structural parameters of stochastic networks with applications to fluid transport in porous materials. *Chemical Engineering Science.* 1988;43:1385-1393.
23. Ljunglöf A. Direct observation of biomolecule adsorption and spatial distribution of functional groups in chromatographic adsorbent particles. PhD Thesis. Center for Surface Biotechnology, Uppsala, Sweden; 2002.
24. Ljunglöf A, Thömmes J. Visualising interparticle protein transport in porous adsorbents by confocal microscopy. *Journal of Chromatography A.* 1998;813:387-395.
25. Bird RB, Stewart WE, Lightfoot EN. *Transport Phenomena*. New York, NY: Wiley; 1960.
26. Cussler EL. *Diffusion. Mass Transfer in Fluid Systems*. Cambridge, UK: Cambridge University Press; 1997.
27. Fournier RL. *Solute Transport in Biological Systems. Basic Transport Phenomena in Biomedical Engineering*. London: Taylor & Francis; 1999.
28. Sutherland WA. Dynamical theory of diffusion for non-electrolytes and the molecular mass of albumin. *The Philosophers' Magazine.* 1905;9:781-785.
29. Renkin EM. Filtration, diffusion and molecular sieving through porous cellulose membranes. *Journal of General Physiology.* 1954;38:225-243.
30. Westrin BA. Diffusion measurements in gels. A methodological study. PhD Thesis. Chem. Eng. 1, Lund University, Lund, Sweden; 1991.
31. Bosma JC, Wesselingh JA. Partitioning and diffusion of large molecules in fibrous structures. *Journal of Chromatography B.* 2000;743: 169-180.
32. Boyer PM, Hsu JT. Experimental studies of restricted protein diffusion in an agarose matrix. *AIChE Journal.* 1992;38:259-272.
33. Masaro L, Zhu XX. Physical models of diffusion for polymer solutions, gels and solids. *Progress in Polymer Science.* 1999;24:731-775.

34. Mattisson C. Diffusion studies in gels using holographic laser interferometry. PhD Thesis. Chem. Eng. 1, Lund University, Lund, Sweden; 1999.
35. Moussaoui M, Benlyas M, Wahl P. Diffusion of proteins in Sepharose Cl-B gels. *Journal of Chromatography*. 1992;591:115-120.
36. Ogston AG, Preston BN, Wells JD. On the transport of compact particles through solution of chain-polymers. *Proceedings of the Royal Society of London.* 1973;A333:297-316.
37. Faxén H. Die Bewegung einer starren Kugel längs der Achse eines mit zäher Flüssigkeit gefüllten Rohres. *Arkiv för Matematik, Astronomi och Fysik*, ISSN 0365-3781, 1923;17:1-28.
38. Ferry JD. Statistical evaluation of sieve constants in ultrafiltration. *Journal of General Physiology*. 1936;20:95-104.
39. Guiochon G, Golshan-Shirazi S, Katti AM. *Fundamentals of Preparative and Nonlinear Chromatography*. London: Academic Press; 1994.
40. Mesquita ME, Vieira e Silva JM. Preliminary study of pH effect in the application of Langmuir and freundlich isoterms to Cu-Zn competitive adsorption. *Geoderma.* 2002;106:219-234.
41. Davis ME. *Numerical Methods and Modeling for Chemical Engineers*. New York, NY: Wiley; 1984.
42. Carlsson F. Mathematical modelling and simulation of fixed-bed chromatographic processes. Tech. Lic. Thesis, Lund University, Lund, Sweden; 1994.
43. Persson P, Kempe H, Zacchi G, Nilsson B. Estimation of adsorption parameters in a detailed affinity chromatography model based on shallow bed experiments. *Process Biochemistry* (2004) in press.
44. Tyn MT, Gusek TW. Prediction of diffusion coefficients of proteins. *Biotechnology and Bioengineering.* 1990;35:327-338.

Manuscript received Dec. 15, 2003, and revision received Mar. 31, 2004.